ELSEVIER

Contents lists available at ScienceDirect

Tribology International

journal homepage: www.elsevier.com/locate/triboint



Effect of peak current on the microstructure, mechanical properties and tribological behavior of Mo_xN coatings deposited by high power impulse magnetron sputtering

Xiaolong Lu^{a,c}, Xudong Sui^{a,b,c,*}, Jian Kang^{a,d}, Xiao Zhang^{a,c}, XingXu Miao^e, Junjie Wang^e, Junying Hao^{a,b,c,*}

- a State Key Laboratory of Solid Lubrication, Lanzhou Institute of Chemical Physics, Chinese Academy of Science, Lanzhou 730000, China
- ^b Center of Materials Science and Optoelectronics Engineering, University of Chinese Academy of Sciences, Beijing 100049, China
- ^c Qingdao Center of Resource Chemistry and New Materials, Qingdao 266000, China
- ^d School of Mechanical and Automotive Engineering, Qingdao University of Technology, Qingdao 266033, China
- ^e Qingdao Zhigaodian Technology Co., Ltd, Qingdao 266037, China

ARTICLE INFO

Keywords: Mo_xN coatings Peak current Tribological behavior Wear rate

ABSTRACT

The Mo_xN coatings are deposited by direct current magnetron sputtering (DCMS) and high power impulse magnetron sputtering (HiPIMS). It is found that the Mo_xN coatings prepared by HiPIMS has a denser microstructure, higher hardness and wear resistance. Besides, the effect of peak current is investigated with respect to the microstructure, mechanical properties and tribological behavior of the coatings. As the peak current increases, the cross-sectional morphology of the coating transforms from featureless to columnar morphology, and the preferred orientation of the coating gradually transfers from (111) to (200). However, the hardness of the coating is not significantly influenced by the peak current. The Mo_xN coating with a peak current of 260 A owns a low friction coefficient of 0.28, which is better than that of the Mo_xN coating prepared by DCMS. The Mo_xN coating with a peak current of 300 A provides excellent wear resistance with the lowest wear rate of 5×10^{-8} mm³/(Nm).

1. Introduction

In the aviation field, the problem of friction and wear has a significant impact on the service life of aero-engine components, such as main shaft bearings and turbine blades [1,2]. The wear caused by harsh service conditions is beyond the performance limits that the substrate can withstand. It is important to emphasize that the surface characteristics of mechanical moving parts are the key issue affecting the tribological performance [3]. In order to enhance the service life of mechanical components, the advancement of coatings with high wear resistance and good adhesion properties has become one of the effective solutions. In particular, new enabling technologies for coating production are also very crucial [3]. For the time being, most coatings are fabricated by vacuum deposition techniques.

Hard coatings are widely used by industry to combat wear in mechanical components, particularly in rolling, rotary and sliding bearing applications. Nitrides and carbides of transition metals stand out among the many hard coatings available today due to their excellent mechanical properties and wear resistance. However, research on nitrides has focused attention on obtaining greater hardness of the coating by attempting to optimize the microstructure. To avoid brittle failure because of cracking, the coatings should also be sufficiently tough and ductile, which can be enhanced by increasing the valence electron concentration of the alloy [4]. In this respect, Mo_xN coating is widely used because of its ability to crystallize in different crystal structures, such as the most reported structures of tetragonal β -Mo₂N, cubic γ -Mo₂N and hexagonal δ -MoN [5]. Besides, Mo_xN coating has high hardness, relatively low friction coefficient and high wear resistance over a wide temperature range, making it one of the candidates for aerospace high temperature lubricating application [5,6].

There are diverse techniques to prepare Mo_xN coatings, including ion beam assisted deposition [6], direct current magnetron sputtering

E-mail addresses: suixudong@licp.cas.cn (X. Sui), jyhao@licp.cas.cn (J. Hao).

^{*} Corresponding authors at: State Key Laboratory of Solid Lubrication, Lanzhou Institute of Chemical Physics, Chinese Academy of Science, Lanzhou 730000, China.

(DCMS) [7], CVD [8], RFMS [9], cathodic arc evaporation [10,11] and PLD [12]. As a new physical vapor deposition technique, the high power impulse magnetron sputtering (HiPIMS) has recently gained widespread research interest [13]. Short high power pulses are imposed on the target in HiPIMS instead of a constant discharge power as in DCMS. This can enhance the probability of electron impact ionization of the sputtered atoms, resulting in the ionization of a large portion of the sputtered material, such as Ti (90%) and Cu (70%) [14]. Therefore, HiPIMS discharges are expected to yield high atomic ionization rates and high energy ions compared to DCMS discharges. In particular, the high density of plasma produced by the highly atomic ionization of the sputtering target results in deposited coatings with dense structure and excellent high adhesion strength [15-18]. To date, several papers have been published on the deposition of Mo_xN coatings by HiPIMS [19–21]. For example, Mei et al. [22] explored the effects of chemical composition on the microstructure, mechanical and tribological properties of Mo-V-Cu-N coatings deposited by HiPIMS, and the coating achieved the lowest friction coefficient ~ 0.3 and wear rate 10^{-17} m³/Nm. The performance of the coating can be further improved by the optimization of process parameters, such as nitrogen partial pressure [21], discharge voltage [20], duty cycle [23,24], pulse frequency [25,26], and pulse length [27,28]. As an important process parameter, the peak current plays an important role in determining the ionization fraction and producing a highly ionized plasma environment [29,30]. The enhancement of the ionization rate leads to intense ion bombardment of the growing coating, which will facilitate the crystallization and densification of the coating [31]. However, too high ion density may lead to the destruction of the coating structure [32]. Therefore, it is necessary to investigate the effect of peak current on the microstructure and properties of coating.

However, scarce studies have been published on the influence of peak currents, especially for the deposition of Mo_xN coatings. The aim of this work is to deposit Mo_xN coatings by HiPIMS technique. Besides, the effect of peak current on microstructure, mechanical and tribological properties of the coatings is explored in detail. In addition, for comparative study, a furnace of Mo_xN samples is also prepared by DCMS in the paper.

2. Experimental details

2.1. Coating deposition

Mo_xN coatings were deposited using a HCMS+CA-400 deposition system with a pure Mo target (483 mm \times 85 mm \times 6 mm, 99.98 at%) connected to the cathode, and Ar and N₂ (99.999 at%) were used as the working gas and reaction gas, respectively. During the reactive deposition, N2 was introduced near the substrate and Ar was introduced into the vacuum chamber from the back of the cathode target to relieve the poisoning of the cathode target after the introduction of the reactive gas. Mirror-polished 9Cr18 steel and Si (100) wafers were provided as substrates. The samples were cleaned by ultrasonication in petroleum ether and anhydrous ethanol, respectively. The process was repeated twice and then the samples were blown dry with a hot air gun and placed in a drying oven. The specific procedure was as follows: the cleaned samples were fixed on the rotating frame, and the vacuum chamber door was closed. When the vacuum level was as low as approximately 3×10^{-3} Pa, the process started to run. Meanwhile, the chamber was heated to 350 °C in order to activate the substrate and enhance the film adhesion. In addition, to get rid of oxide layers and other adsorbed impurities on the substrate surface, all substrates were first etched with Ar⁺ for 20 min (argon flow: 150 sccm, bias voltage: -850 V). The substrates were then further etched and cleaned using the arc-light electron source enhanced glow discharge (AEG) plasma cleaning function with the cathode AEG current set to 70 A, the anode AN current set to 35 A and the bias voltage set to 300 V. Afterwards, the Mo transition layer was prepared in 10 min under an Ar gas flow rate of 60 sccm to improve the film-based adhesion strength. Next, N2 was introduced under a gas flow rate of 15 sccm and

the Mo_vN coating was deposited by controlling the peak currents of 180 A, 220 A, 260 A and 300 A for 2 h. The specific preparation details were presented in Table 1. For subsequent discussion, the samples deposited at various peak currents were labeled as S180, S220, S260 and S300, respectively. For the purpose of comparing the influences of the microstructure and properties of the coatings prepared by HiPIMS, a separate furnace of Mo_xN samples was prepared by DCMS in this study. The DC sputtering current of the Mo source was fixed at 4 A, and the coating was deposited at a working pressure of 0.39 Pa. The pulse voltage (U_{out}) and target current (I_{out}) waveforms on different pulse time are shown in Fig. 1. It is obvious that the output value of the Mo target peak current is significantly different within a pulse time period (0-300 μ s), while the output value of the pulse voltage is almost the same. The output current values shown in Fig. 1 are analog and are linear function values about the actual current. Therefore, the current values do not display actual units.

2.2. Coating characterization

The surface and cross-sectional morphology of the coatings were observed using a scanning electron microscope (JSM-7610 F). The surface morphology, roughness and particle sizes of the coatings were analyzed using atomic force microscopy (Bruker Dimension Icon). The crystalline phase structure of MoxN coatings was analyzed using a highresolution X-ray diffractometer (D8 ADVANCE) in grazing incidence mode (incidence angle of 1°). Further microstructural details of the coatings were obtained by high resolution transmission electron microscope (FEI Talos F200s). TEM samples were prepared from steel substrates using a focused ion beam (Strata 400 S). XPS (ESCALAB 250xi) was utilized to determine surface chemistry of deposited coatings. The monochromatic Al Ka X-ray radiation with kinetic energy of 1486.8 eV was used and the electron emission angle was 30°. The spot size of analyzed area was 400 µm. Prior to XPS analyses, the sputter was performed by Ar⁺ etching ion gun at an etching rate of 17.4 nm/min and etching time of 2 min. The Ar⁺ energy was 1000 eV and the incidence angle was 45°. The XPS was performed under a base pressure of 3.0×10^{-7} mbar. Charge compensation was implemented using a low voltage electron flood gun. XPS was used to observe the distribution of elements in the sample. The elastic modulus and hardness of the coatings were measured by a nanoindenter (STEP E400). The maximum indentation load ranges from 7 to 9 mN with a Berkovich tip diamond indenter. In our work, the hardness and elastic modulus of the coating were measured five times to ensure the accuracy of the data, and the final average of the five sets of data was taken. In addition, the variance obtained by averaging the five data sets was taken as the error bars. The residual stress of coatings was determined by film stress tester (FST 1000). To ensure the reliability of the data, the average and variance of the three measured values were obtained. So as to evaluate the filmbased adhesion strength, a scratch test was performed by scratch tester (MFT-4000). And the scratches were observed by optical microscope (NMM-800TRF). To evaluate the tribological properties of Mo_xN coatings, a friction test was conducted using a friction and wear tester

Table 1 The deposition parameters of Mo_xN coating deposited by HiPIMS.

Parameters	Values
Working pressure (Pa)	0.33
Bias voltage (V)	-120
Argon flow (SCCM)	60
Nitrogen flow (SCCM)	15
Deposition temperature (°C)	350
Peak current (A)	180/220/260/300
Frequency (Hz)	100
Pulse width (μs)	300
Duty cycle	3%
Deposition time (min)	120

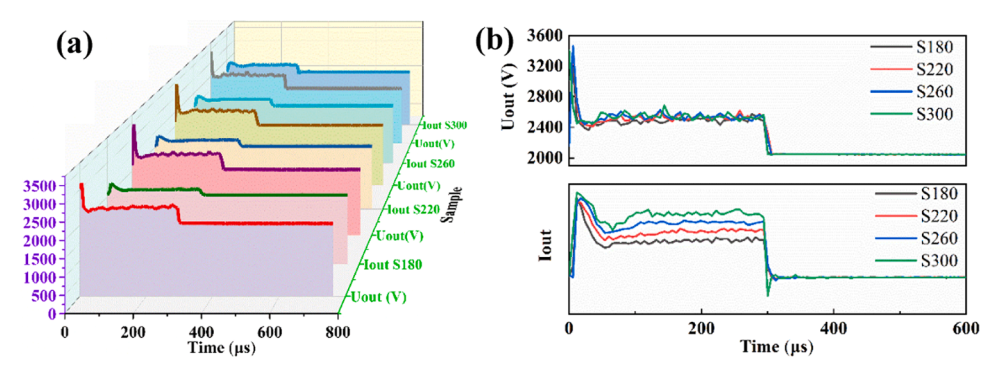


Fig. 1. Variation of pulse voltage (Uout) and target current (Iout) with pulse time.

(CSM, TRB³) against an Al_2O_3 counterpart with a diameter of 6 mm. The tribological testing parameters including the normal load (5 N), the sliding frequency (5 Hz), the sliding stroke (6 mm), the total sliding stroke (216 m) and the sliding time (1 h), had been maintained constant throughout the experiment. In addition, wear profiles were observed by a 3D surface profiler (UP-Sigma) and the wear rate was calculated [33].

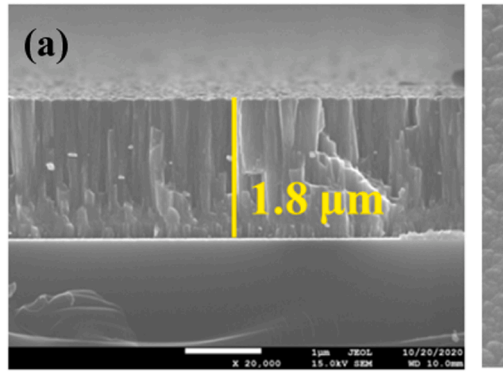
3. Results and discussion

3.1. Structure and morphology

The structure of the cross-section and surface of the Mo_xN coatings deposited by DCMS and HiPIMS are given in Fig. 2 and Fig. 3, respectively. The MoxN coatings prepared by the DCMS exhibit a loose columnar morphology. However, the Mo_xN coating prepared by HiPIMS has a denser structure and smooth surface. This indicates that the highenergy bombardment during HiPIMS leads to the densification of the coating and the smoothing of the coating surface. At low peak currents, the S180 coating does not exhibit a significant columnar morphology and the particle aggregation on the coating surface is not obvious. However, as the peak current increases, the microstructure of the coating appears columnar morphology and the particles on the surface start to agglomerate. It is suggested that the increased ionization rate brought about by raising the peak current leads to intense ion bombardment of the growing coating, which promotes the crystallization of the coating. The maximum thickness of the S180 coating is $1.2~\mu m$, while the thickness of the coating varies between $0.79~and~1~\mu m$ as the peak current increases. This indicates that the effect of peak current on coating thickness is not completely linearly correlated. In general, the thickness of the coatings deposited at higher peak currents is less than that of the coatings deposited at lower peak currents. This can be attributed to the increased ionization rate resulting in intense ion bombardment of the growing coating, which promotes the densification of the coating.

The three-dimensional morphology of the coatings ($5 \times 5 \ \mu m^2$ area) and the corresponding roughness are shown in Fig. 4. As shown in Fig. 4, the Mo_xN coatings deposited by DCMS are distributed with many protrusions on the surface and have the largest roughness of 5.83 nm. The Mo_xN coatings prepared by HiPIMS have a more homogeneous distribution of particles on the surface, and the roughness is slightly lower than that of the Mo_xN-DC coatings. The roughness of the Mo_xN coating decreases with the increase of peak current. In addition, the particle size of the prepared coating shown in Fig. 5 is also obtained from the three-dimensional morphology of the coating. The Mo_xN-DC coating exhibits the particle size of 0.101 μ m. Compared to Mo_xN-DC coatings, the particle size of the deposited Mo_xN coating becomes smaller at lower peak currents, while the particle size of the coating becomes larger at higher peak currents.

Fig. 6 shows the XRD patterns of the Mo_xN coatings. It is shown that the Mo_xN coatings prepared by DCMS are mainly composed of hexagonal δ -MoN phase. As can be seen from the Fig. 6, the coatings deposited by HiPIMS exhibit four effective diffraction peaks after excluding the effect of the substrate. The diffraction peaks at 37.3°, 43.2°, 62.9°, and 75.5° correspond to the (111), (200), (220), and (311) crystallographic planes of the face-centered cubic γ-Mo₂N phase (JCPDF 25–1366), respectively. This indicates that the coatings exist mainly in the facecentered cubic y-Mo₂N phase structure [34]. In general, the peak deviation of all exhibited Mo-N peaks compared to the JCPDF data can be observed due to the presence of residual stresses within the coating [35]. As shown in the Fig. 6, the intensity of the γ-Mo₂N (111) diffraction peak tends to increase and then decrease with the gradual increase of the peak current. And the preferred orientation of the coating gradually changes from Mo₂N (111) to Mo₂N (200). The competition for the preferred orientation of (111) and (200) is driven by the strong isotropy of potential energy and diffusivity of the moving surface species. At low ion-to-metal flux ratios, the (111) surface provides more stable cation sites than the (200) surface, resulting in a net cation flux for the shift in orientation from (200) to (111) oriented grains [36,37]. However, a net



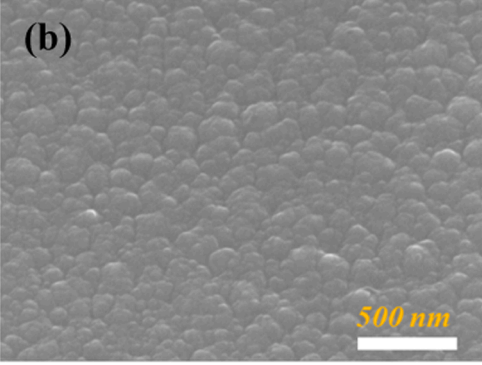


Fig. 2. Cross-sectional and surface morphology of Mo_xN coatings deposited by DCMS.

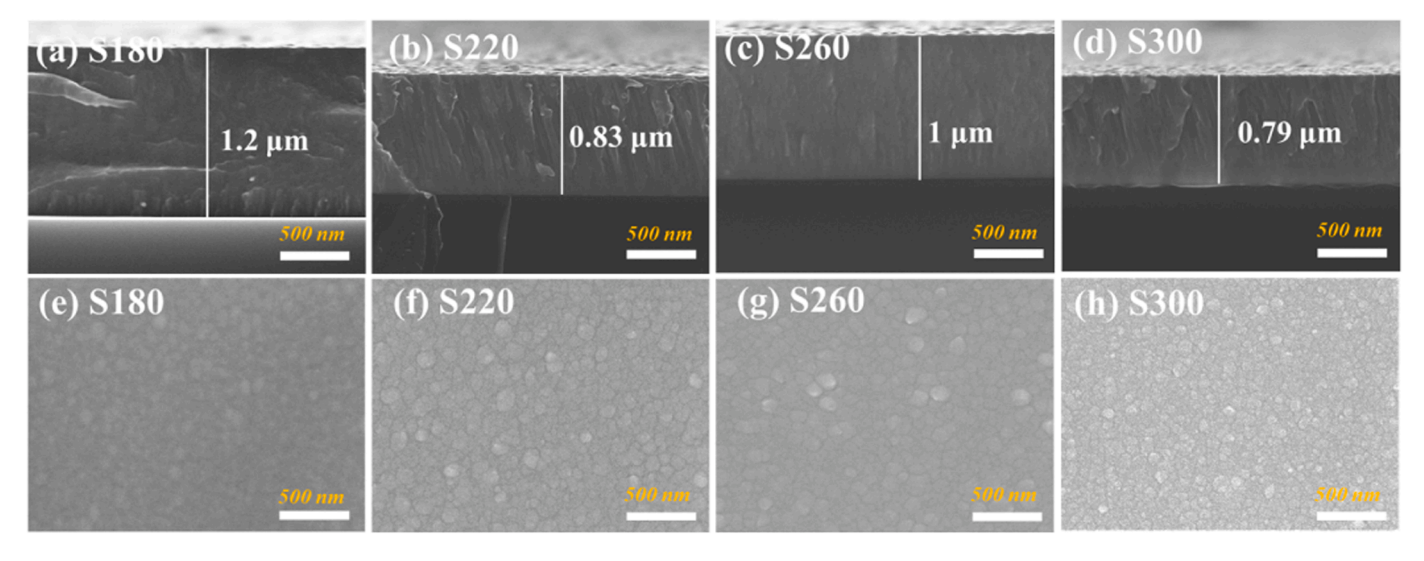


Fig. 3. Cross-sectional and surface morphology of Mo_xN coatings deposited by HiPIMS.

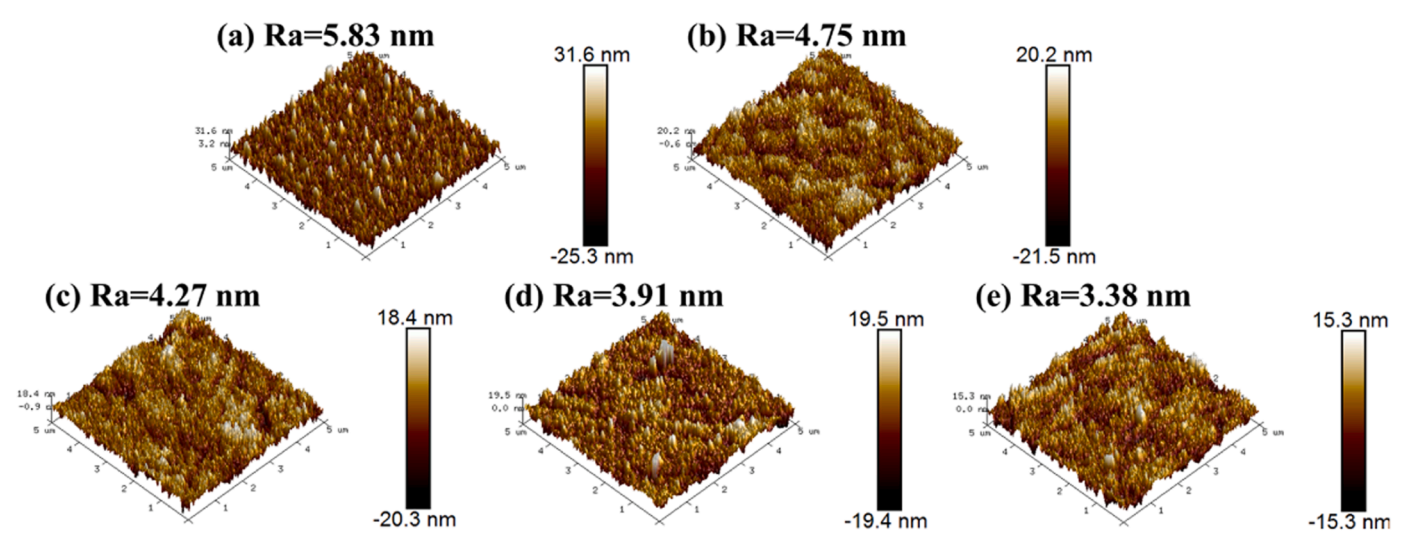


Fig. 4. AFM images and the corresponding roughness of Mo_xN coatings (a) Mo_xN-DC, (b) S180, (c) S220, (d) S260, and (d) S300.

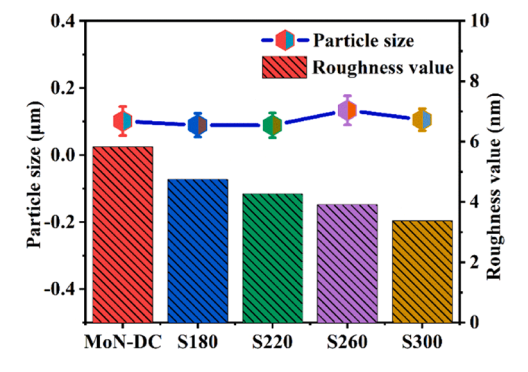


Fig. 5. The roughness values and particle sizes of Mo_xN coatings.

cation flux can be reversed at high ion-to-metal flux ratios. The evolution of the preferred direction from (111) to (200) with increasing ion-to-metal flux ratio is attributed to the kinetic control [38,39].

Besides, an increase of peak current favours the formation of Mo_2N (220) crystal plane. The apparent $\gamma\text{-}Mo_2N$ (220) surface diffraction peak is due to the strong ion bombardment by the higher peak current, and

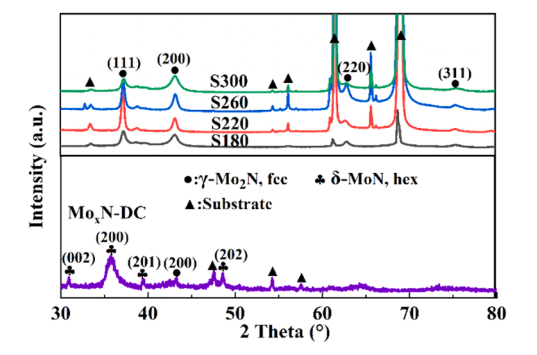


Fig. 6. XRD patterns of Mo_xN coatings.

the "channel effect" occurs under the high energy ion bombardment, which induces the (220) plane to grow along the coating surface [40].

To further determine the microstructure of the Mo_xN coatings, cross-sectional TEM micrographs and corresponding HRTEM images of the S260 sample are shown in Fig. 7. Fig. 7a presents the columnar structure along the direction of coating growth. As shown in Fig. 7b, the lattices

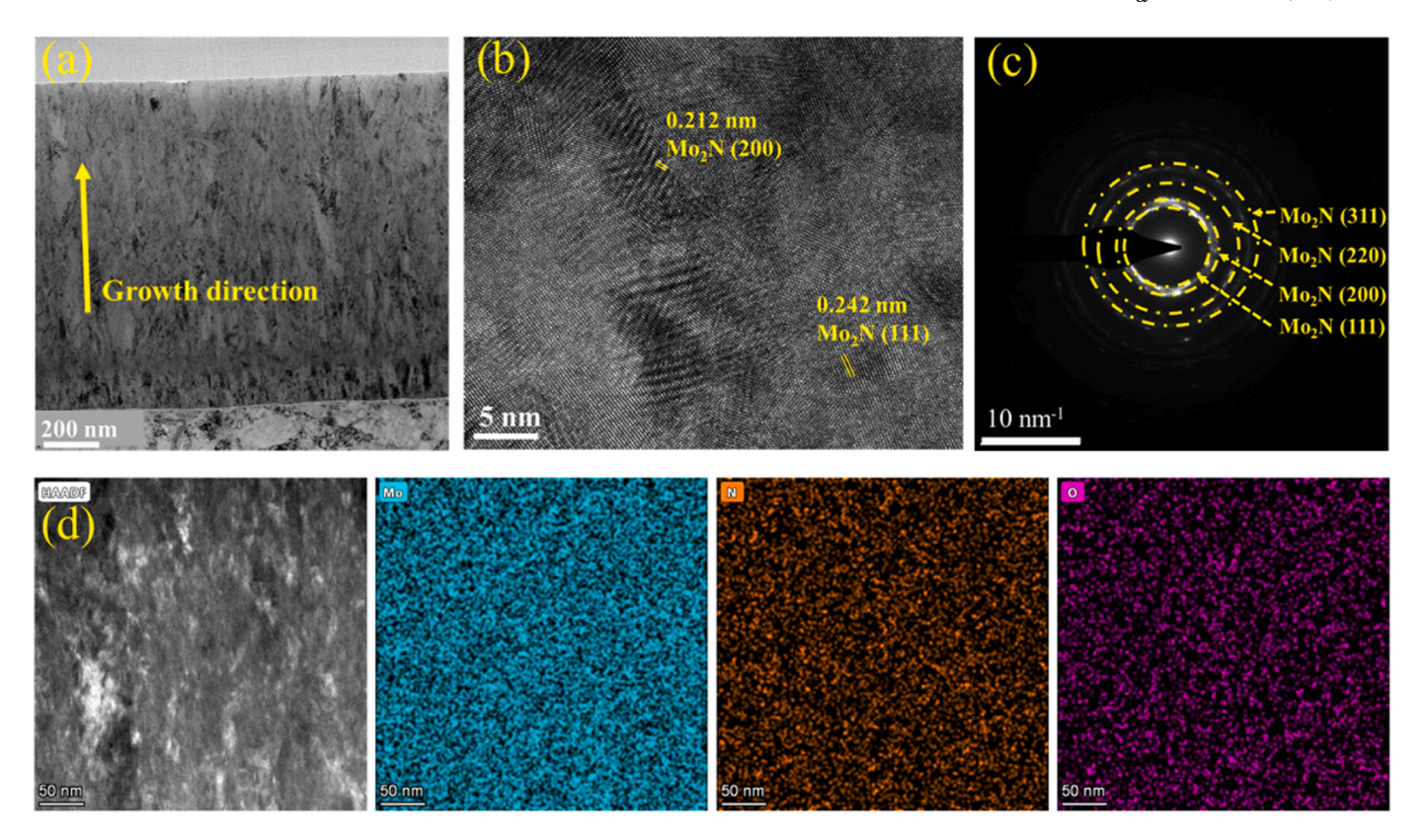


Fig. 7. Cross-sectional TEM micrographs of Mo_xN coatings: (a) TEM micrographs, (b) HRTEM, (c) SAED pattern and (d) HAADF image with STEM elements mappings.

with spacings of 0.242 nm and 0.212 nm are recognized and considered to be $\gamma\text{-Mo}_2N$ (111) and (200) planes in the high-resolution image of the Mo_xN coating. The Mo_2N (111), Mo_2N (200), Mo_2N (220) and Mo_2N (311) planes from selected area electron diffraction (SAED) can be recognized, indicating that Mo_2N is the main phase of the coating, consistent with the XRD results. In addition, Mo, N and O elements in the Mo_xN coatings are uniformly distributed in the coatings by EDS analysis.

XPS is used to observe the elemental content of the coating. Fig. 8 shows the elemental composition of the Mo_xN coatings. From the figure, it can be observed that the Mo_xN coating prepared by DCMS has a low Mo content and a high N content. However, Mo_xN coatings prepared by HiPIMS show a higher Mo content due to higher Mo ionization. In addition, as the peak current increases, the Mo element content of the coating increases in small increments. Therefore, increasing the peak current will increase the population of Mo ion species. The N element content fluctuates between 63.71 at% and 68.83 at%, which accounts for more than half of the entire coating element.

The chemical bonding and electronic structure of the Mo_xN coating are investigated by XPS analysis. Surprisingly it is found that for thin

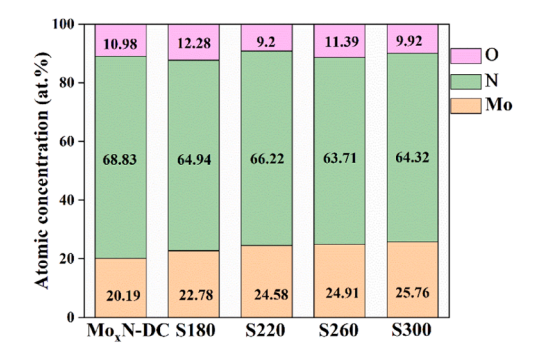


Fig. 8. Chemical compositions (at%) of the samples.

film samples composed of metals, nitrides, carbides, borides, oxides and oxynitrides, the C1s peak position E_B^F varies over a wide range from 284.08 to 286.74 eV [41,42]. Consequently, the use of C1s peak at the charge reference is not reliable. The sum $E_B^F + \phi_{SA}$ is essentially constant at 289.58 \pm 0.14 eV, where the E_B^F is the binding energy of the C1 s peak referenced to the Fermi level, and the ϕ_{SA} is work function [43–45]. Therefore, the referencing to C1s should be calibrated by 289.58 eV ϕ_{SA} .

As presented in Fig. 9, the full spectra of the Mo_xN coating are mainly composed of Mo 3d, N 1 s, and O 1 s. The Mo 3d, N 1 s, and O 1 s spectra of Mo_xN coatings deposited by DCMS and HiPIMS are shown in Fig. 10a-e. For the Mo_xN coating deposited by DCMS (Fig. 10a), the fitted curves of the Mo 3d spectra show clear two doublets, indicating that the different binding energies (BE) correspond to the mutual binding between Mo and the other elements. The peaks at binding energies of

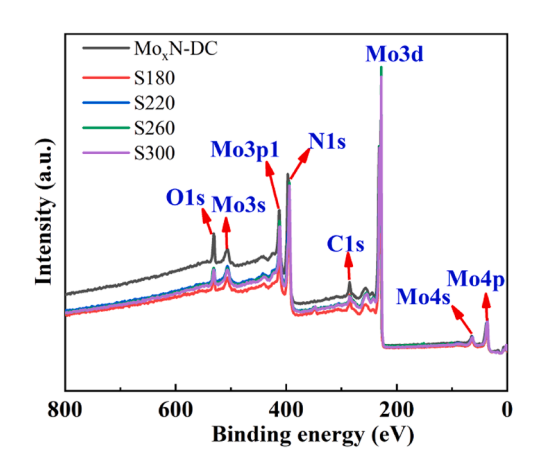


Fig. 9. XPS full spectra of the MoxN coating.

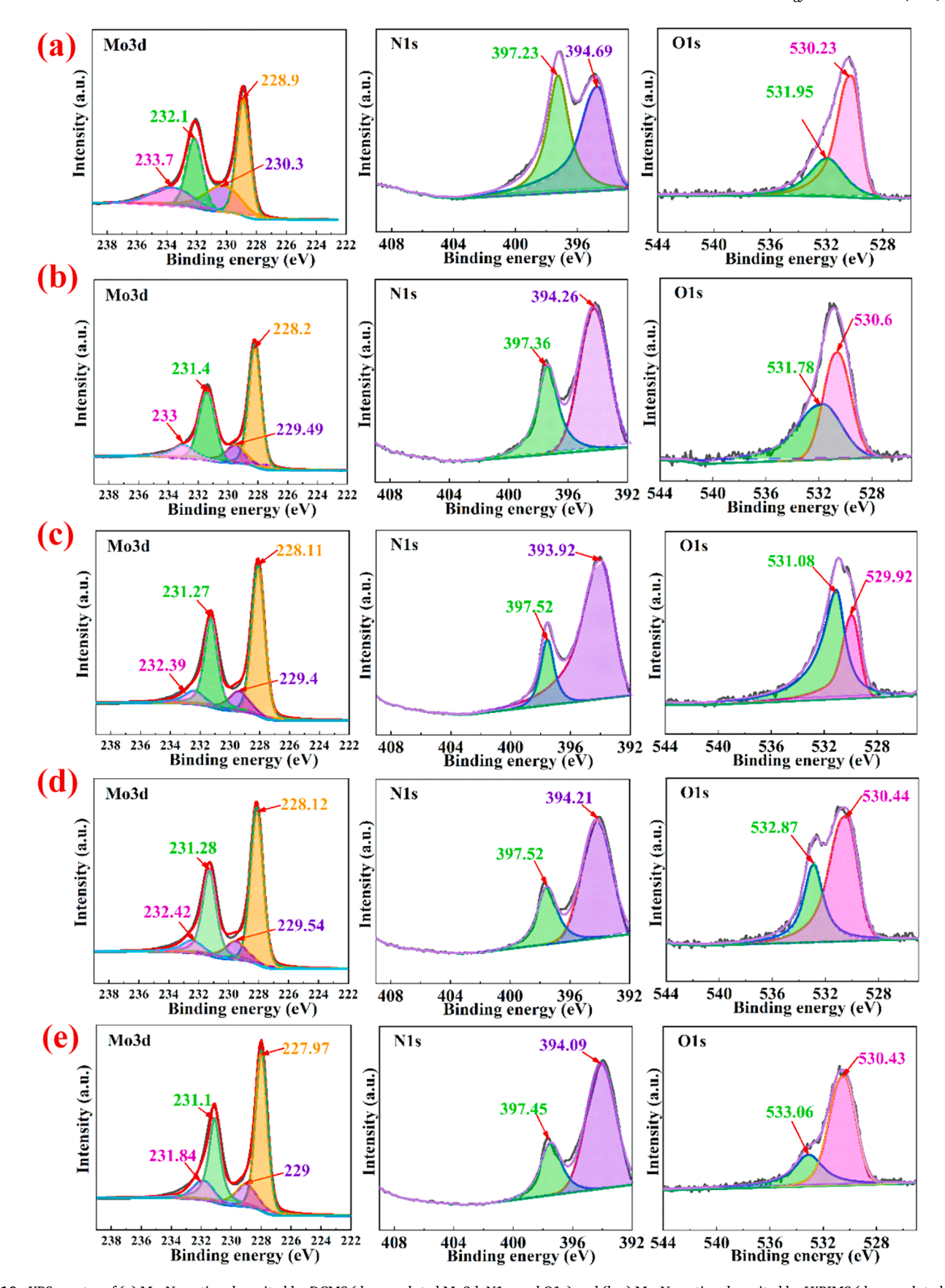


Fig. 10. XPS spectra of (a) Mo_xN coating deposited by DCMS (deconvoluted Mo3d, N1s, and O1s) and (b-e) Mo_xN coating deposited by HiPIMS (deconvoluted Mo3d, N1s, and O1s).

228.9 eV and 232.1 eV are allocated to the Mo 3d_{5/2} and Mo 3d_{3/2}, corresponding to the formation of Mo-N bonding [19,21]. In addition, the Mo $3d_{5/2}$ and Mo $3d_{3/2}$ of Mo⁴⁺ species observed at 230.3 eV and 233.7 eV representing the presence of MoO2, which is due to the formation of surface oxides from exposure to the atmosphere [46]. The N1s spectra can be decomposed into two binding states corresponding to Mo 3p (BE=394.69 eV) and N 1 s (BE=397.23 eV) [46]. The fitted curves of the O 1 s spectra for Mo_xN coating displays the fitted peaks 530.23 eV and 531.95 eV attributed to the presence of Mo-O bonding formation and oxygen as surface impurities, respectively [47]. Similar peaks of the Mo-N bonding in the Mo and N regions are also observed in the XPS spectra of Mo_xN coatings deposited by HiPIMS, as shown in Fig. 10b-e. However, for the coatings deposited by HiPIMS, the Mo 3d peak shifts to a lower BE, indicating a change in the chemical valence state of Mo. The coatings deposited by DCMS exhibit mainly MoN phase structure. However, the coatings deposited by HiPIMS are mainly present in the face-centered cubic γ-Mo₂N phase structure. This suggests that the use of HiPIMS is able to increase the population of ionic species compared to the DCMS preparation, leading to more Mo ions dissociated and bound to N, which leads to a change in the chemical state of Mo. For the XPS spectra of the \$180 coating (Fig. 10b), the fitted Mo 3d binding energy peaks at 229.49 eV and 233 eV correspond to the Mo⁴⁺ (3d_{5/2}) and Mo^{4+} (3d_{3/2}), respectively [46]. The states of Mo^{4+} (BE=229.4 eV, 232.39 eV), Mo⁴⁺ (BE=229.54 eV, 232.42 eV) and Mo⁴⁺ (BE=229 eV, 231.84 eV) are shown in the Mo 3d spectra (Fig. 10c-e), respectively.

3.2. Mechanical properties

Hardness (H) and Young's modulus (E) as well as the combination index (H/E or H³/E²) are able to predict the wear resistance of the coating to some extent [48]. The hardness and elastic modulus of Mo_xN coatings deposited by DCMS (MoxN-DC) and HiPIMS are given in Fig. 11a. As shown in Fig. 11a, the hardness and elastic modulus values of the Mo_xN coatings deposited by DCMS are 22.2 GPa and 321.8 GPa, respectively. However, the hardness and modulus values of MoxN coatings prepared by HiPIMS ranges from 29.59 to 32.54 GPa and from 330.7 to 343.7 GPa, respectively. This is because the coatings prepared by DCMS show a loose columnar morphology, resulting in a low hardness of the coating. In contrast, the Mo_xN coatings prepared by HiPIMS have a denser microstructure, which in turn provides excellent mechanical properties. At lower peak current, the S180 sample shows the highest hardness and elastic modulus values of 32.5 GPa and 343.7 GPa, respectively. However, the hardness and elastic modulus of the coatings deposited at higher peak currents are slightly lower. This is probably due to the fact that higher peak currents favor the crystallinity of the coatings, allowing the coatings to reappear with columnar morphology, which affects the mechanical properties of the coatings.

The coatings deposited by HiPIMS generally indicate high wear resistance due to their typically high hardness and modulus values. In Fig. 11b, the H/E and ${\rm H}^3/{\rm E}^2$ values of ${\rm Mo_xN}$ coatings deposited by DCMS and HiPIMS are calculated for comparison. The H/E ratio is defined as

the energy absorbed by the coating before failure and $\mathrm{H}^3/\mathrm{E}^2$ is a reflection of the coating's ability to resist plastic deformation [49,50]. It is observed that the $\mathrm{Mo_xN}$ coatings prepared by DCMS show relatively low H/E and $\mathrm{H}^3/\mathrm{E}^2$ values of 0.069 and 0.106, respectively, which implies a lower resistance to plastic deformation in response to external mechanical contact forces. However, the H/E and $\mathrm{H}^3/\mathrm{E}^2$ values of $\mathrm{Mo_xN}$ coatings prepared by HiPIMS are high, ranging from 0.087 to 0.095 and 0.227–0.292, respectively. Among them, the coatings (S180 and S300) deposited at lower and higher peak currents have higher H/E and $\mathrm{H}^3/\mathrm{E}^2$ values, which indicates that the $\mathrm{Mo_xN}$ coatings deposited in this case exhibit good wear resistance and resistance to plastic deformation.

The scratch resistance of the MoxN coatings are tested by a scratch tester, and the surface morphologies of the scratch scars are observed with an optical microscope. Generally speaking, LC1 refers to the beginning of cracking at the edge of the scratch, indicating cohesive failure in the coating. L_{C2} refers to the beginning of chipping failure extending from the arc tensile cracks, indicating adhesive failure between the coating and the substrate. As the normal load increases further, the cracks become more severe, eventually causing the coating to flake off and expose the substrate. Therefore, a higher critical load L_{C3}, indicating the complete adhesion failure between the coating and the substrate, is used. The positions of L_{C1} , L_{C2} and L_{C3} on each track of the coatings are indicated. The Mo_xN-DC sample shows a lower L_{C1}, L_{C2} and L_{C3} about 11 N, 22 N and 62.5 N, respectively. However, the Mo_xN coatings deposited by HiPIMS own a better scratch resistance than that of Mo_xN-DC coatings. For example, a higher L_{C1} of 15.9 N and L_{C2} of 30 N and a highest L_{C3} of 77 N are recorded for S180 coating. As the loading force increases, a small number of transverse cracks first appear inside the scratch, then more intensive arc-shaped transverse cracks appear, and flaking occurs on both sides of the scratch, and eventually the coating is completely flaked off on the substrate, exposing the substrate. There exist a lot of arc-shaped transverse cracks inside the scratch and spallation along the scratch track sides for the Mo_xN-DC sample. However, the cracks in the scratch of the Mo_xN coatings deposited by HiPIMS are the finest and there is no obvious large flaking in the entire scratch track. This indicates that the Mo_xN coatings prepared by HiPIMS have higher adhesion strength than those prepared by DCMS. Fig. 12.

Deposition of coatings in a vacuum environment is susceptible to intrinsic residual stresses and depends on process variables such as deposition temperature, gas pressure and deposition power [51]. Fig. 13 shows the residual stresses in the Mo_xN coatings prepared by DCMS and HiPIMS. It can be found that the Mo_xN coatings prepared via DCMS exhibit a low compressive residual stress (-1.54~GPa). However, the Mo_xN coatings prepared via HiPIMS owns higher residual stresses. The coatings prepared by DCMS have a loose columnar microstructure, so the residual stresses caused by sputtering may be released, leading to a lower compressive stress. However, the coatings prepared by HiPIMS show higher compressive stress due to a more compact structure. Besides, the coatings grown during HiPIMS preparation are bombarded by a large number of high-energy ions and more Ar ions are generated in the HiPIMS afterglow. The Ar $^+$ bombardment leads to higher

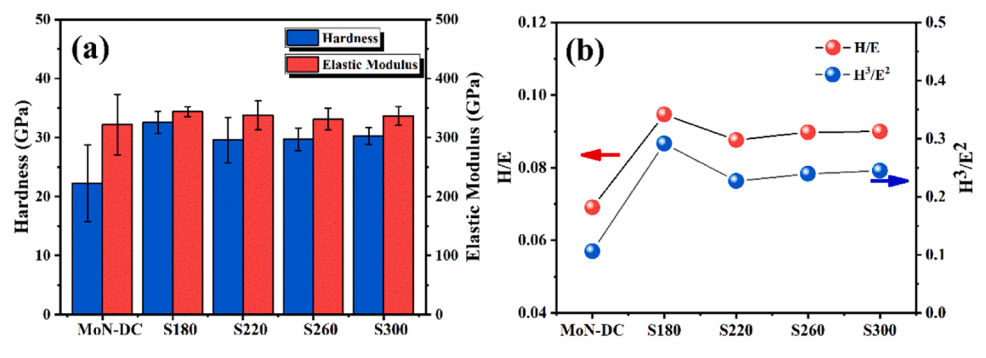


Fig. 11. (a) Hardness and elastic modulus and (b) H/E and H³/E² of Mo_xN coatings.

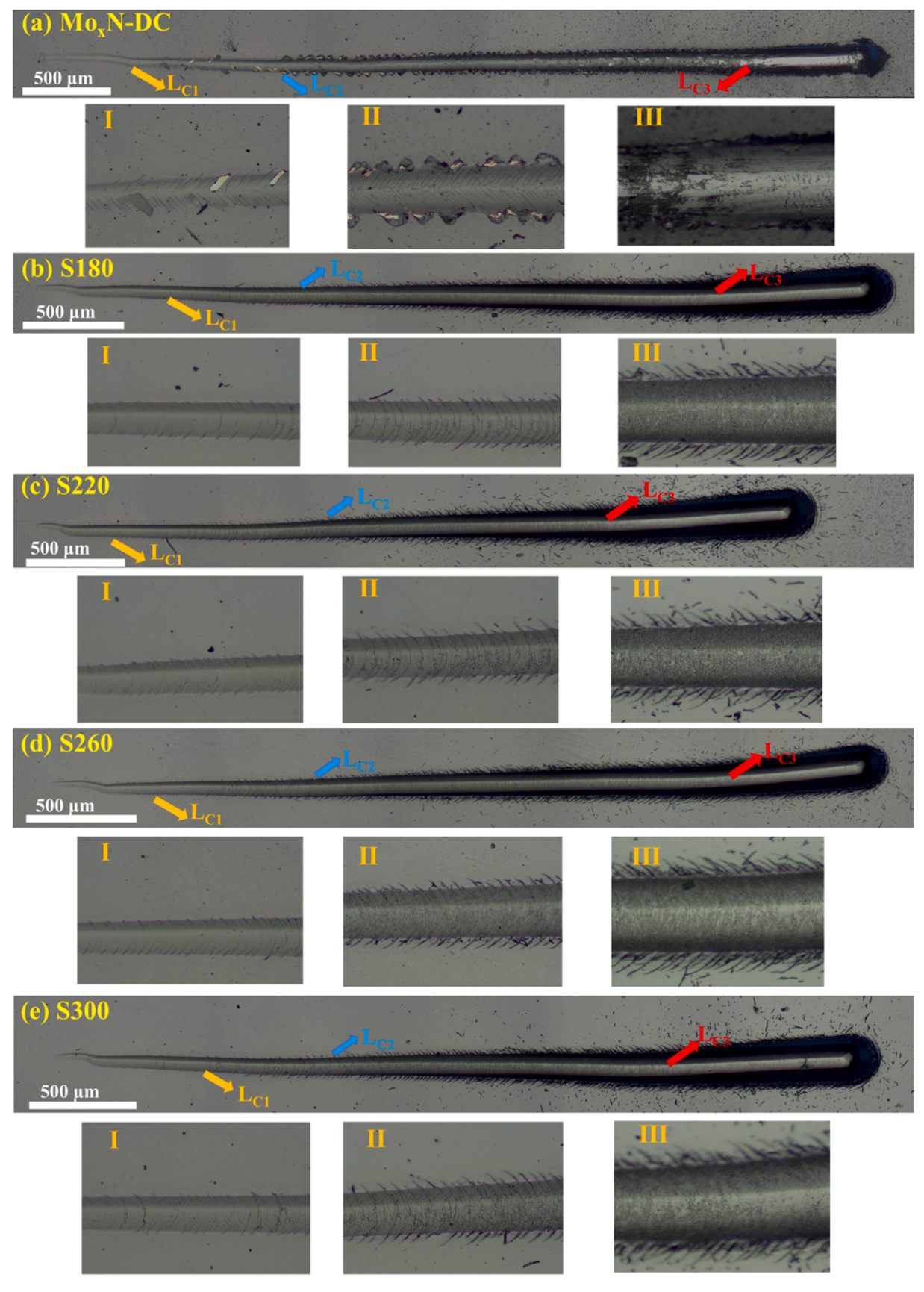


Fig. 12. Scratch images in the Mo_xN coatings.

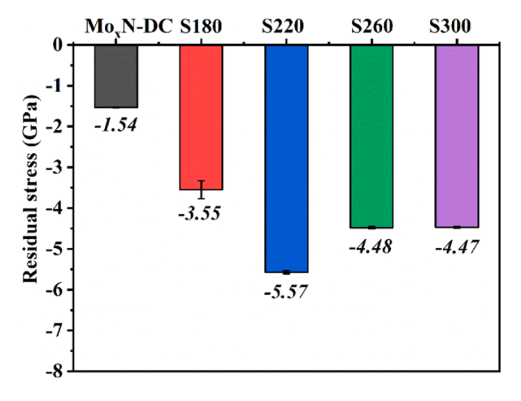


Fig. 13. Residual stress of MoxN coatings.

compressive stresses in the coatings [52]. Therefore, the higher ionization fraction in HiPIMS results in higher compressive residual stresses compared to DCMS [53].

3.3. Tribological properties

The friction coefficient curves of the deposited Mo_xN coatings are given in Fig. 14a. As shown in the figure, the average value of friction coefficient for Mo_xN coating deposited by DCMS in the atmospheric environment is approximately 0.49, and the friction coefficient curve fluctuates widely. However, the friction coefficient curves of all coatings deposited by HiPIMS have a relatively smooth state. Among them, the friction coefficients of S180, S220 and S300 coatings are not very different, all around 0.4. The MoxN coating with a peak current of 260 A gives an extremely low friction coefficient of 0.28, which is better than that of the Mo_xN coating prepared by DCMS. The results of tribological tests confirm that the friction coefficient of Mo_xN coatings prepared by DCMS is relatively high, but slightly lower for HiPIMS preparation. Similarly reported, e.g., Fenker et al. [54] fabricated Mo_xN coatings by DCMS and HiPIMS and found that the highest friction coefficient of 0.55 was measured for the dc-0.4 sample compared to roughly 0.4 for both HiPIMS deposited ones.

Fig. 14b shows the wear rate of Mo_xN coatings. As shown in Fig. 14b, the wear rate of the Mo_xN coating prepared by DCMS is 2×10^{-7} mm³/(Nm), which is significantly larger than that prepared by HiPIMS. This is because the Mo_xN coating prepared by DCMS has a loose structure and low hardness, which leads to a higher wear rate of the coating. However, the peak current shows little effect on the wear rate of the Mo_xN coatings prepared by HiPIMS. It is noteworthy that the wear rate of Mo_xN coatings prepared at lower and higher peak currents is lower, with the S300 coating having the lowest wear rate of 5×10^{-8} mm³/(Nm). This can be related to the higher H/E and H³/E² values of the coatings deposited at lower and higher peak currents (S180 and S300). The load-bearing

capacity and resistance to plastic deformation of the coatings are higher under such conditions, and the wear resistance of the coatings is improved.

As illustrated in Fig. 15, the three-dimensional wear profiles of Mo_xN coatings are analyzed. It can be observed from Fig. 15 that the Mo_xN coatings prepared by DCMS have wider and deeper wear tracks, indicating a higher wear rate. However, the wear tracks of the coatings prepared by HiPIMS are relatively narrow and shallow, which means that better wear resistance can be obtained. Besides, the S180 coating has a deeper wear depth of about $0.25\,\mu m$, and its wear behavior is dominated by downward loading forces. However, the maximum wear depth of the S220 coating is reduced (0.16 µm), but its wear width increases and its wear behavior extends to both sides. In the same way as the S220 coating, the S260 coating wear trajectory expands to both sides, which is responsible for its large wear rate. Although the S260 coating has deeper grooves appearing due to the peeling abrasive particles, the overall wear depth is the shallowest at about 0.05 µm. It can also be observed that the S300 coating has a wear depth of about 0.16 µm, and its wear behavior is dominated by downward loading forces, which is consistent with the wear behavior of the S180 coating.

Fig. 16 shows the plots of friction coefficient, wear rate and H/E, and the wear width, wear depth and H/E for Mo_xN coatings. As the lower modulus of elasticity disperses the applied load over a wider range, the coating achieves better wear resistance. Higher H/E $({\rm H}^3/{\rm E}^2)$ values are used as an important indicator of greater resistance to plastic deformation. It can be seen that the coatings prepared by HiPIMS have high H/E values with shallower wear depths and smaller wear widths than the Mo_xN coatings prepared by DCMS, resulting in superior wear resistance.

The reason for the enhanced wear resistance of the Mo_xN coating prepared by HiPIMS is shown schematically in Fig. 17. The coatings prepared by DCMS have a loose structure and are less dense, leading to coatings with poor mechanical properties and wear resistance. The Mo_xN coatings prepared by DCMS have a low adhesion strength, in addition, the lower resistance to plastic deformation affects the degree of brittle tensile cracking of the coating, which in turn leads to the removal of the coating from the scratch. In contrast, Mo_xN coatings prepared by HiPIMS technology have a dense structure and more interfaces inside the coating. As a result, coatings prepared with HiPIMS show higher compressive residual stresses. The high compressive stress leads to coatings with high hardness values, resulting in coatings with increased wear resistance.

4. Conclusions

The Mo_xN coatings are prepared by DCMS and HiPIMS technique, and the microstructure, mechanical and tribological properties of Mo_xN coatings are systematically analyzed. More specifically,

(1) The Mo_xN-DC coatings exhibit a loose columnar morphology.

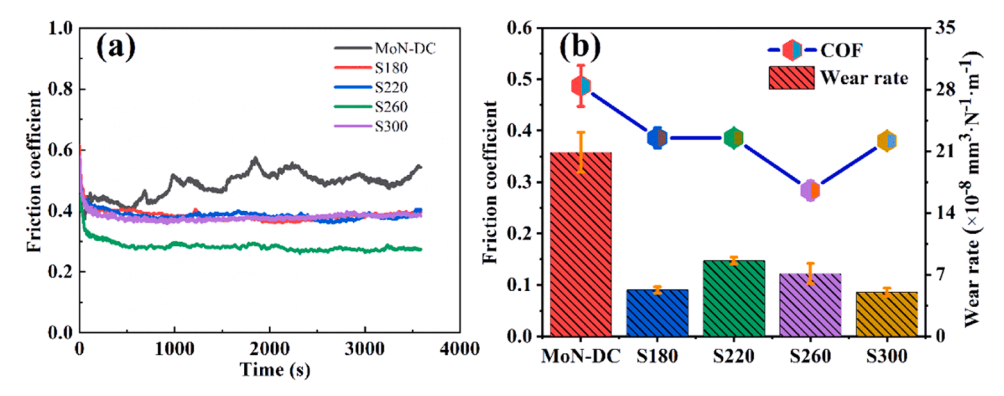


Fig. 14. (a) Friction coefficient curves and (b) wear rates of the Mo_xN coatings.

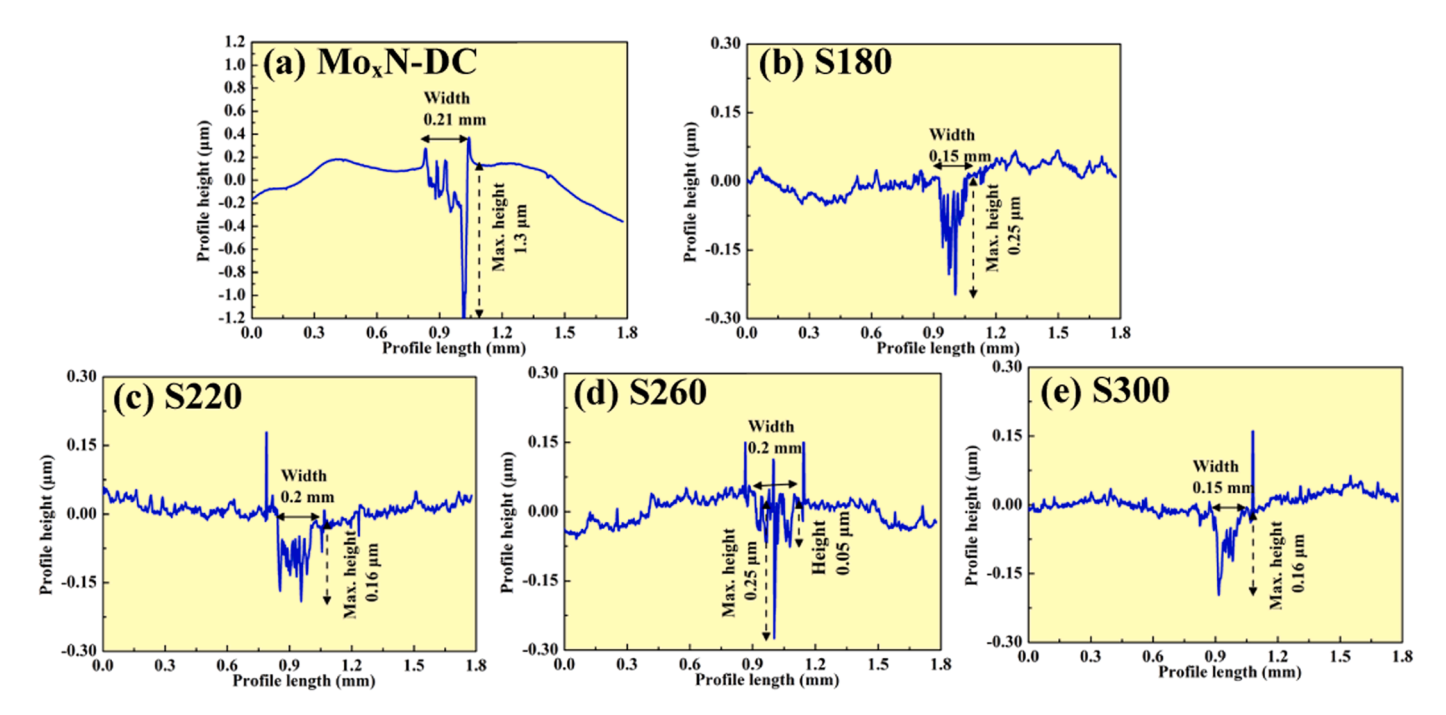


Fig. 15. Three-dimensional profile height of Mo_xN coatings.

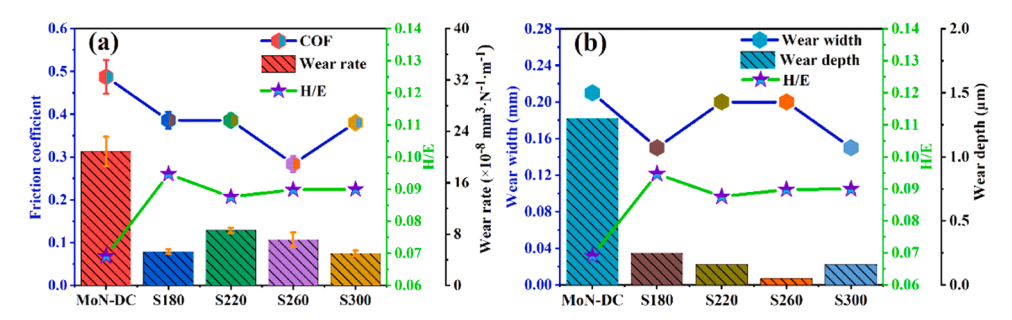


Fig. 16. Plots of (a) friction coefficient, wear rate and H/E; and (b) wear width, wear depth and H/E for Mo_xN coatings.

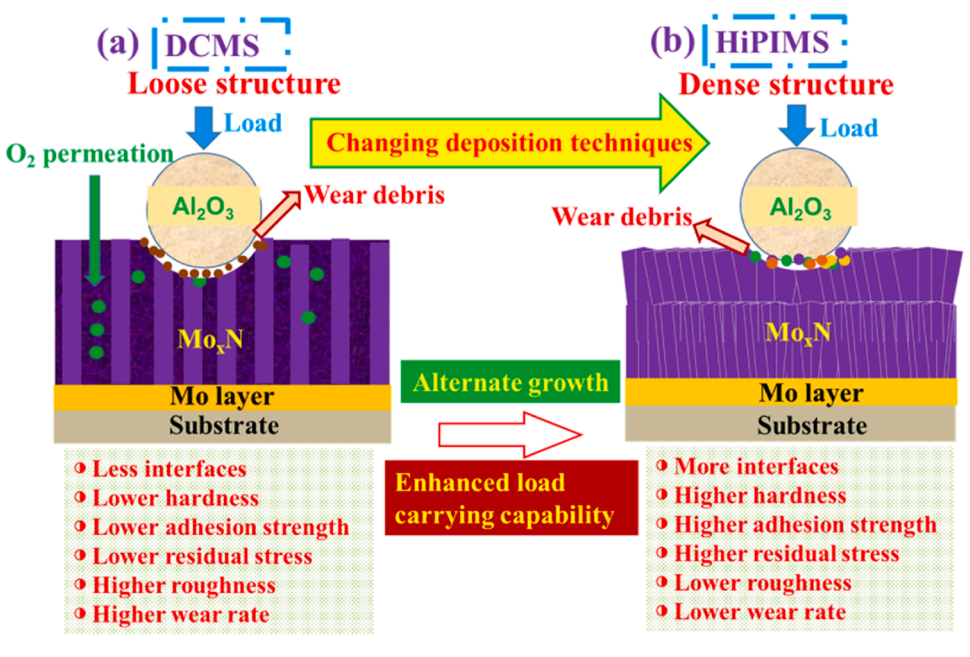


Fig. 17. Schematic diagram to display the reasons for the enhanced wear resistance of Mo_xN coatings prepared by HiPIMS.

However, the Mo_xN coating prepared by HiPIMS has a denser morphology and smooth surface. The Mo_xN -DC coatings are mainly composed of hexagonal δ -MoN phase. Whereas a FCC γ -Mo $_2N$ phase is easy to form in the coatings deposited by HiPIMS, due to the high populations of ionic species.

- (2) Compared to Mo_xN -DC coatings, Mo_xN coatings prepared by HiPIMS show higher adhesion strength, compressive residual stress, hardness, and H/E (H^3/E^2) ratios.
- (3) Thanks to the dense structure and excellent mechanical properties, the wear rate of the ${\rm Mo_xN}$ coatings deposited by HiPIMS is an order of magnitude lower than that of the ones deposited by DCMS. By tuning the peak current, the coating deposited at 300 A owns the lowest wear rate of about 5×10^{-8} mm³/(Nm), while an extremely low friction coefficient of about 0.28 is achieved by the coating deposited at 260 A.

Declaration of Competing Interest

The authors declare that they have no known competing financial interests or personal relationships that could have appeared to influence the work reported in this paper.

Data availability

Data will be made available on request.

Acknowledgments

The authors gratefully acknowledge the financial support of the Strategic Priority Research Program of the Chinese Academy of Sciences (XDB0470000), the National Natural Science Foundation of China (51835012, 51975554), the Basic Research Projects (2020-JCJQ-ZD-155-12), the Natural Science Foundation of Gansu Province (22JR5RA111) and the project of improving the innovation ability of scientific and technological SMEs in Shandong Province (2022TSGC1128).

Statement of originality

We declare the following statements:

- (1) The article is original.
- (2) The article has been written by the stated authors who are ALL aware of its content and approve its submission.
 - (3) The article has not been published previously.
 - (4) The article is not under consideration for publication elsewhere.
- (5) No conflict of interest exists, or if such conflict exists, the exact nature must be declared.
- (6) If accepted, the article will not be published elsewhere in the same form, in English or in any other language, without the written consent of the Publisher.

References

- Hetmanczyk M, Swadzba L, Mendala B. Advanced materials and protective coatings in aero-engines application. J Ach Mater Manuf Eng 2007;24:372–81.
- [2] Espallargas N, Berget J, Guilemany JM, Benedetti AV, Suegama PH. Cr₃C₂-NiCr and WC-Ni thermal spray coatings as alternatives to hard chromium for erosioncorrosion resistance. Surf Coat Technol 2008;202:1405–17.
- [3] Zin V, Miorin E, Deambrosis SM, Montagner F, Fabrizio M. Mechanical properties and tribological behaviour of Mo-N coatings deposited via high power impulse magnetron sputtering on temperature sensitive substrates. Tribol Int 2018;119: 322-80
- [4] Yu W, Li H, Li JL, Liu ZL, Huang JW, Kong J, et al. Balance between oxidation and tribological behaviors at elevated temperatures of Hf_{1-x}W_xN films by optimizing W content. Vacuum 2023:207:111673
- [5] Krysina OV, Ivanov YuF, Koval NN, Prokopenko NA, Shugurov VV, Petrikova EA, et al. Composition, structure and properties of Mo-N coatings formed by the method of vacuum-arc plasma-assisted deposition. Surf Coat Technol 2021;416: 127153.

- [6] Zhu XD, Yue D, Shang C, Fan MT, Hou B. Phase composition and tribological performance of molybdenum nitride coatings synthesized by IBAD. Surf Coat Technol 2013;228:S184–9.
- [7] Xu X, Su FH, Li ZJ. Microstructure and tribological behaviors of MoN-Cu nanocomposite coatings sliding against Si₃N₄ ball under dry and oil-lubricated conditions. Wear 2019;434–435:202994.
- [8] Roberson SL, Finello D, Davis RF. Growth of Mo_xN films via chemical vapor deposition of $MoCl_5$ and NH_3 . Surf Coat Technol 1998;102:256–9.
- [9] Anitha VP, Major S, Chandrashekharam D, Bhatnagar M. Deposition of molybdenum nitride thin films by rf reactive magnetron sputtering. Surf Coat Technol 1996;79:50–4.
- [10] Gilewicz A, Jedrzejewski R, Kochmanska A, Warcholinski B. Structure of MoCN films deposited by cathodic arc evaporation. Thin Solid Films 2015;577:94–6.
- [11] Yang Q. Wear resistance and solid lubricity of molybdenum-containing nitride coatings deposited by cathodic arc evaporation. Surf Coat Technol 2017;332: 283–95.
- [12] Inumaru K, Baba K, Yamanaka S. Synthesis and characterization of superconducting β-Mo₂N crystalline phase on a Si substrate: an application of pulsed laser deposition to nitride chemistry. Chem Mater 2005;17:5935–40.
- [13] Gudmundsson JT. The high power impulse magnetron sputtering discharge as an ionized physical vapor deposition tool. Vacuum 2010;84:1360–4.
- [14] Alami J, Bolz S, Sarakinos K. High power pulsed magnetron sputtering: Fundamentals and applications. J Alloy Compd 2009;483:530–4.
- [15] Elmkhah H, Attarzadeh F, Fattah-alhosseini A, Kim KH. Microstructural and electrochemical comparison between TiN coatings deposited through HIPIMS and DCMS techniques. J Alloy Compd 2018;735:422–9.
- [16] Tiron V, Velicu IL, Cristea D, Lupu N, Stoian G, Munteanu D. Influence of ion-to-neutral flux ratio on the mechanical and tribological properties of TiN coatings deposited by HiPIMS. Surf Coat Technol 2018;352:690–8.
- [17] Kozak T, Vlcek J, Kos S. Transport and ionization of sputtered atoms in high-power impulse magnetron sputtering discharges. J Phys D Appl Phys 2013;46:105203.
- [18] Kuo CC, Lin YT, Chan A, Chang JT. High temperature wear behavior of titanium nitride coating deposited using high power impulse magnetron sputtering. Coatings 2019;9:555.
- [19] Mei HJ, Wang R, Zhong X, Dai W, Wang QM. Influence of nitrogen partial pressure on microstructure and tribological properties of Mo-Cu-V-N composite coatings with high Cu content. Coatings 2018;8:24.
- [20] Mei HJ, Ding JC, Zhao JF, Wang T, Huang KJ, Guo ZH, et al. Effect of charge voltage on the microstructural, mechanical, and tribological properties of Mo-Cu-V-N nanocomposite coatings. Coatings 2021;11:1565.
- [21] Mei HJ, Zhao SS, Wu ZT, Dai W, Wang QM. Effect of nitrogen partial pressure on microstructure and mechanical properties of Mo-Cu-V-N composite coatings deposited by HIPIMS. Surf Coat Technol 2017;329:68–76.
- [22] Mei HJ, Luo QS, Huang XL, Ding JC, Zhang TF, Wang QM. Influence of lubricious oxides formation on the tribological behavior of Mo-V-Cu-N coatings deposited by HIPIMS. Surf Coat Technol 2019;358:947–57.
- [23] Hsiao YC, Lee JW, Yang YC, Lou BS. Effects of duty cycle and pulse frequency on the fabrication of AlCrN thin films deposited by high power impulse magnetron sputtering. Thin Solid Films 2013;549:281–91.
- [24] Chang CL, Shih SG, Chen PH, Chen WC, Ho CT, Wu WY. Effect of duty cycles on the deposition and characteristics of high power impulse magnetron sputtering deposited TiN thin film. Surf Coat Technol 2014;259:232–7.
- [25] Nedfors N, Mockute A, Palisaitis J, Persson POÅ, Näslund LÅ, Rosen J. Influence of pulse frequency and bias on microstructure and mechanical properties of TiB₂ coatings deposited by high power impulse magnetron sputtering. Surf Coat Technol 2016;304:203–10.
- [26] Dai W, Kwon SH, Wang QM, Liu JM. Influence of frequency and C₂H₂ flow on growth properties of diamond-like carbon coatings with AlCrSi co-doping deposited using a reactive high power impulse magnetron sputtering. Thin Solid Films 2018:647:26–32.
- [27] Jing FJ, Yin TL, Yukimura K, Sun H, Leng YX, Huang N. Titanium film deposition by high-power impulse magnetron sputtering: influence of pulse duration. Vacuum 2012:86:2114–9.
- [28] Bagcivan N, Bobzin K, Grundmeier G, Wiesing M, Ozcan O, Kunze C, et al. Influence of HPPMS pulse length and inert gas mixture on the properties of (Cr,Al) N coatings. Thin Solid Films 2013;549:192–8.
- [29] Zuo X, Chen RD, Liu JZ, Ke PL, Wang AY. The influence of superimposed DC current on electrical and spectroscopic characteristics of HiPIMS discharge. AIPAdv 2018;8:015132.
- [30] Hsu YH, Wu WY. Antibacterial Ag-Cu coatings deposited using an asymmetric bipolar high-power impulse magnetron sputtering technique. Surf Coat Technol 2019;362:302–10.
- [31] Nouvellon C, Michiels M, Dauchot JP, Archambeau C, Laffineur F, Silberberg E, et al. Deposition of titanium oxide films by reactive high power impulse magnetron sputtering (HiPIMS): influence of the peak current value on the transition from metallic to poisoned regimes. Surf Coat Technol 2012;206:3542–9.
- [32] Wu WY, Chan MY, Hsu YH, Chen GZ, Liao SC, Lee CH, et al. Bioapplication of TiN thin films deposited using high power impulse magnetron sputtering. Surf Coat Technol 2019;362:167–75.
- [33] Lu XL, Yan MM, Yan Z, Chen WY, Sui XD, Hao JY, et al. Exploring the atmospheric tribological properties of MoS₂-(Cr, Nb, Ti, Al, V) composite coatings by high throughput preparation method. Tribol Int 2021;156:106844.
- [34] Tan YT, Zhu YL, Li HB. Construction of Mo₂N nanoparticles embedded in N, O-doped carbon sheets and its supercapacitive behaviors. J Alloy Compd 2023;946: 169458.

- [35] Gassner G, Mayrhofer PH, Kutschej K, Mitterer C, Kathrein M. Magnéli phase formation of PVD Mo-N and W-N coatings. Surf Coat Technol 2006;201:3335–41.
- [36] Shin C-S, Gall D, Kim Y-W, Hellgren N, Petrov I, Greene JE. Development of preferred orientation in polycrystalline NaCl-structure δ-TaN layersgrown by reactive magnetron sputtering: role of low-energy ion surface interactions. J Appl Phys 2002;92:5084.
- [37] Gall D, Kodambaka S, Wall MA, Petrov I, Greene JE. Pathways of atomistic processes on TiN(001) and (111) surfaces during film growth: an ab initio study. J Appl Phys 2003;93:9086.
- [38] Alling B, Steneteg P, Tholander C, Tasnádi F, Petrov I, Greene JE, et al. Configurational disorder effects on adatom mobilities on Ti_{1-x}Al_xN (001) surfaces from first principles. Phys Rev B 2012;85:245422.
- [39] Greene JE, Sundgren J-E, Hultman L. Development of preferred orientation in polycrystalline TiN layers grown byultrahigh vacuum reactive magnetron sputtering. Appl Phys Lett 1995;67:2928.
- [40] Ma CH, Huang JH, Chen H. Texture evolution of transition-metal nitride thin films by ion beam assisted deposition. Thin Solid Films 2004;446:184–93.
- [41] Greczynski G, Hultman L. C 1s peak of adventitious carbon aligns to the vacuum level: dire consequences for material's bonding assignment by photoelectron spectroscopy. Chem Phys Chem 2017;18:1507–12.
- [42] Greczynski G, Hultman L. Reliable determination of chemical state in x-ray photoelectron spectroscopy based on sample-work-function referencing to adventitious carbon: resolving the myth of apparent constant binding energy of the C 1s peak. Appl Surf Sci 2018;451:99–103.
- [43] Greczynski G, Hultman L. Compromising science by ignorant instrument calibration—need to revisit half a century of published XPS data. Angew Chem 2020;132:5034–8.
- [44] Greczynski G, Hultman L. X-ray photoelectron spectroscopy: towards reliable binding energy referencing. Prog Mater Sci 2020;107:100591.

- [45] Greczynski G, Hultman L. The same chemical state of carbon gives rise to two peaks in X-ray photoelectron spectroscopy. Sci Rep 2021;11(1):5.
- [46] Wang T, Zhang GJ, Ren S, Jiang BL. Effect of nitrogen flow rate on structure and properties of MoN_x coatings deposited by facing target sputtering. J Alloy Compd 2017;701:1–8.
- [47] Kumar DD, Hazra S, Panda K, Kuppusami P, Stimpel-Lindner T, Duesberg GS. Probing the impact of tribolayers on enhanced wear resistance behavior of carbon-rich molybdenum-based coatings. ACS Appl Mater Interfaces 2022;14:26148–61.
- [48] Liu YC, Liang BH, Huang CR, Wu FB. Microstructure evolution and mechanical behavior of Mo-Si-N films. Coatings 2020;10:987.
- [49] Shao WT, Wu SK, Yang W, He JH, Lu SD, Xu DP, et al. Effect of modulation period on microstructure and mechanical properties of (AlSiTiVNbCr)N/(AlSiTiVNbCr)CN nano-multilayer films. Vacuum 2023;207:111660.
- [50] Leyland A, Matthews A. On the significance of the H/E ratio in wear control: a nanocomposite coating approach to optimised tribological behavior. Wear 2000; 246:1–11
- [51] Pappacena KE, Singh D, Ajayi OO, Routbort JL, Erilymaz OL, Demas NG, et al. Residual stresses, interfacial adhesion and tribological properties of MoN/Cu composite coatings. Wear 2012;278–279:62–70.
- [52] Cemin F, Abadias G, Minea T, Lundin D. Tuning high power impulse magnetron sputtering discharge and substrate bias conditions to reduce the intrinsic stress of TiN thin films. Thin Solid Films 2019;688:137335.
- [53] Xu Y, Li Gd, Li G, Gao FY, Xia Y. Effect of bias voltage on the growth of super-hard (AlCrTiVZr)N high-entropy alloy nitride films synthesized by high power impulse magnetron sputtering. Appl Surf Sci 2021;564:150417.
- [54] Fenker M, Balzer M, Kellner S, Polcar T, Richter A, Schmidl F, et al. Formation of solid lubricants during high temperature tribology of silver-doped molybdenum nitride coatings deposited by dcMS and HIPIMS. Coatings 2021;11:1415.